Electronic Supplementary Material (ESI) for RSC Advances.

Supporting Information for

Photoisomerization and Thermal isomerization of Ruthenium Aqua Complexes with Chloro Substituted Asymmetric Bidentate Ligands

Masanari Hirahara*[†], Hiroki Goto[†], Rei Yamamoto[†], Masayuki Yagi[§], and Yasushi Umemura[†]

[†] Department of Applied Chemistry, School of Applied Science, National Defense Academy of Japan, Hashirimizu 1-10-20, Yokosuka, Kanagawa, 239-8686, Japan

[§] Department of Materials Science and Technology, Faculty of Engineering, Niigata University, 8050 Ikarashi-2, Niigata 950-2181, Japan

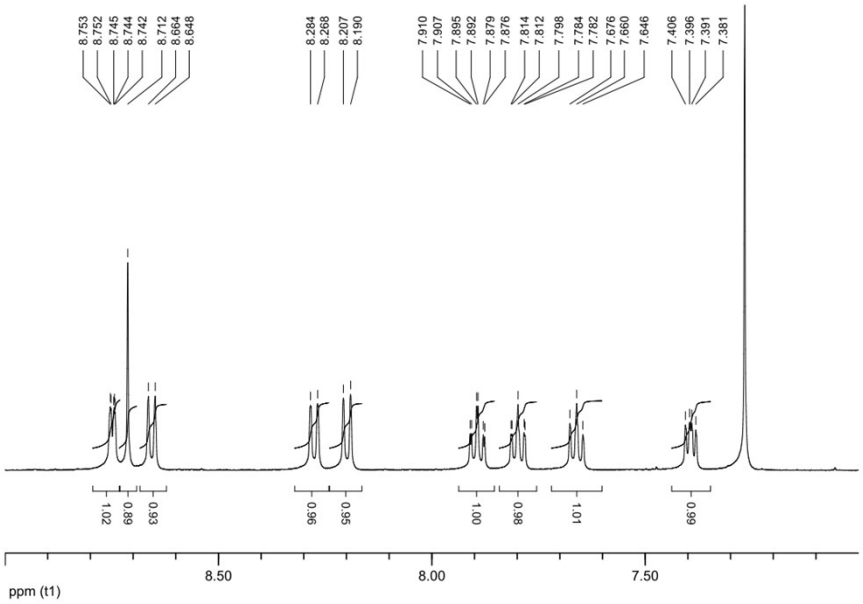

Figure S1A ^{1}H NMR spectrum of 2-(2'-pyridyl)-4-chloroquinoline in $CDCl_3$.

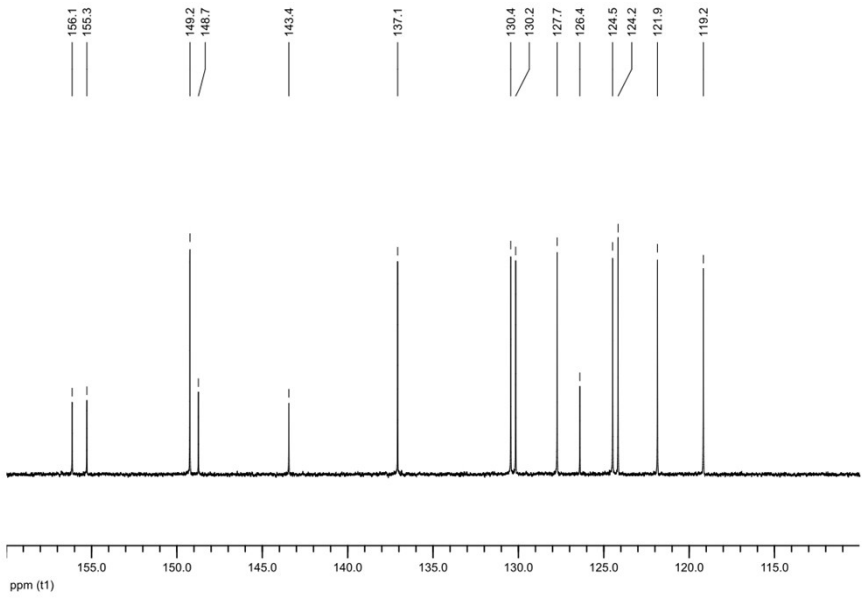

Figure S1B. ^{13}C NMR spectrum of 2-(2'-pyridyl)-4-chloroquinoline in $CDCl_3$.

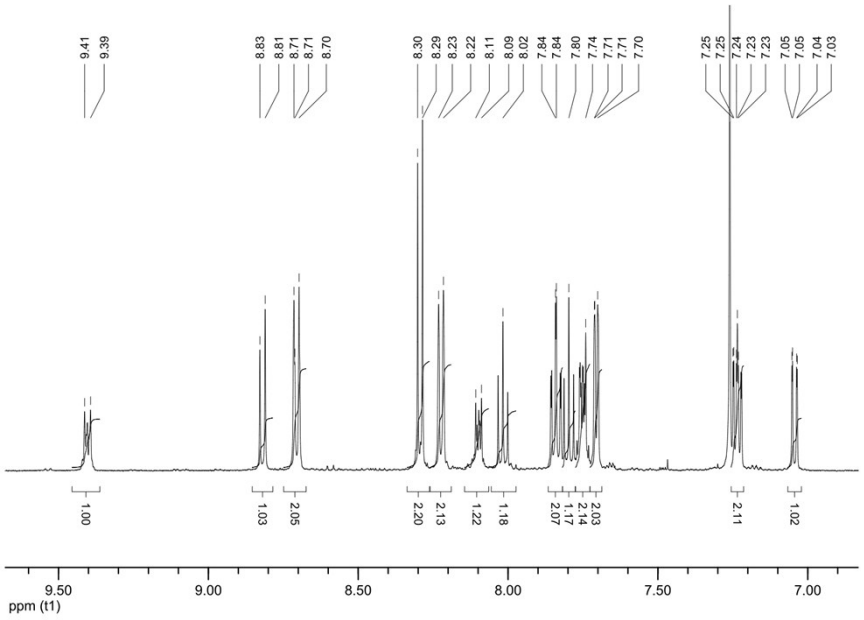

Figure S2A. ^{1}H NMR spectrum of *p*-[**2Cl**]Cl in CD_3OD (10%) and $CDCl_3$ (90%).

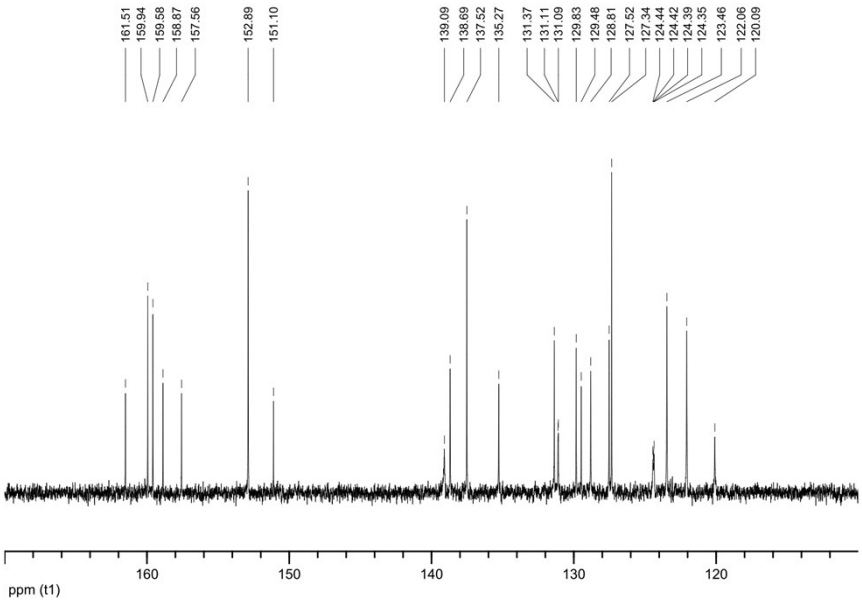

Figure S2B. ^{13}C NMR spectrum of *p*-[**2Cl**]Cl in CD_3OD (10%) and $CDCl_3$ (90%).

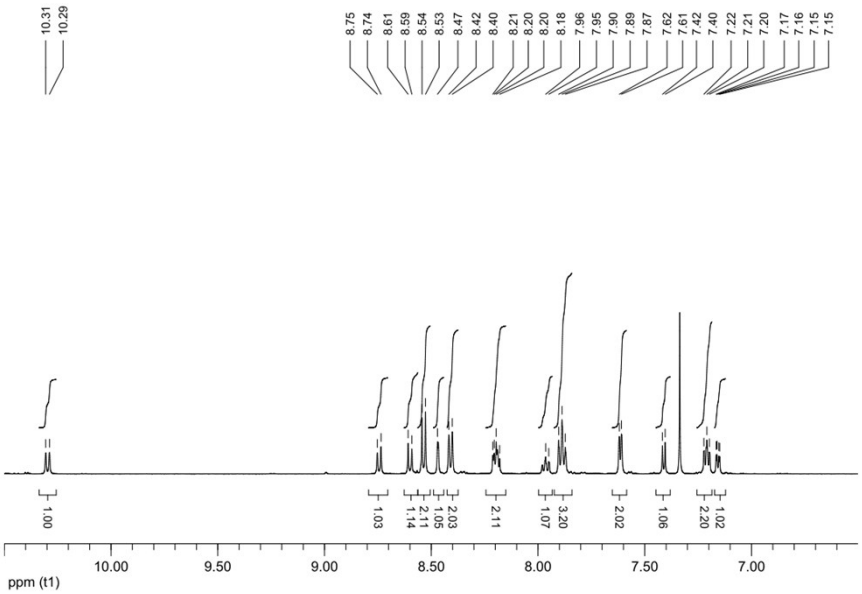

Figure S3A. ^{1}H NMR spectrum of *p*-[**3Cl**]Cl in CD_3OD (10%) and $CDCl_3$ (90%).

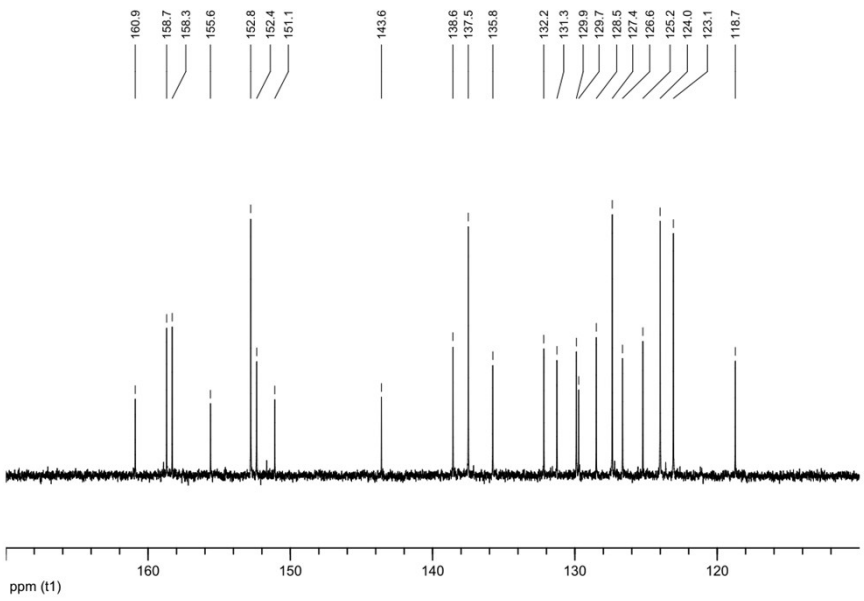

Figure S3B. ^{13}C NMR spectrum of *p*-[**3Cl**]Cl in CD_3OD (10%) and $CDCl_3$ (90%).

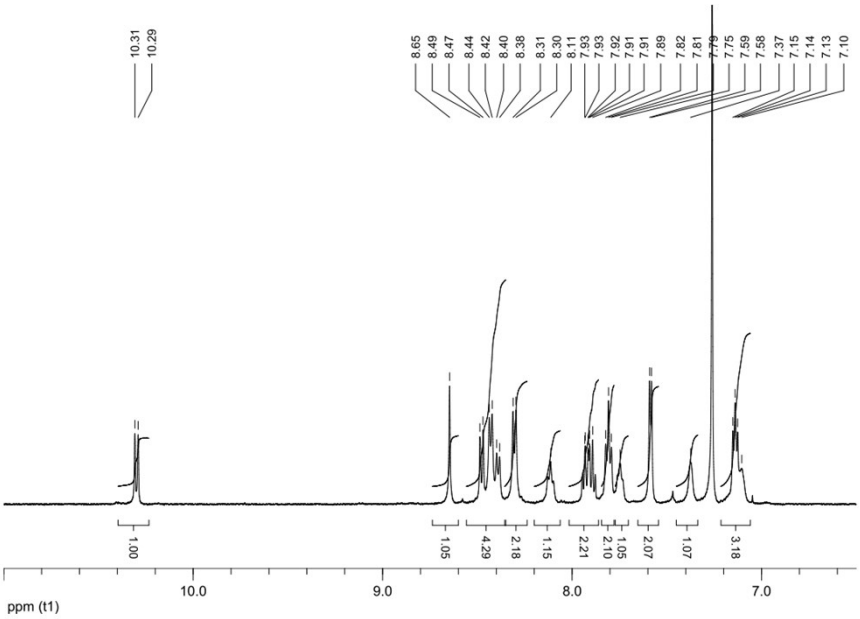

Figure S4A. ^{1}H NMR spectrum of *p*-[**4Cl**]Cl in CD_3OD (10%) and $CDCl_3$ (90%).

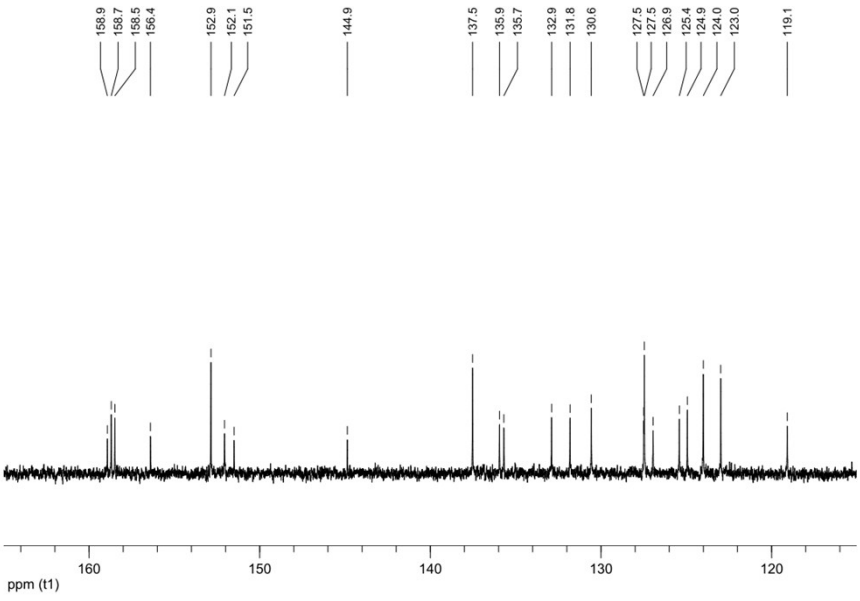

Figure S4B. ^{13}C NMR spectrum of *p*-[**4Cl**]Cl in CD_3OD (10%) and $CDCl_3$ (90%).

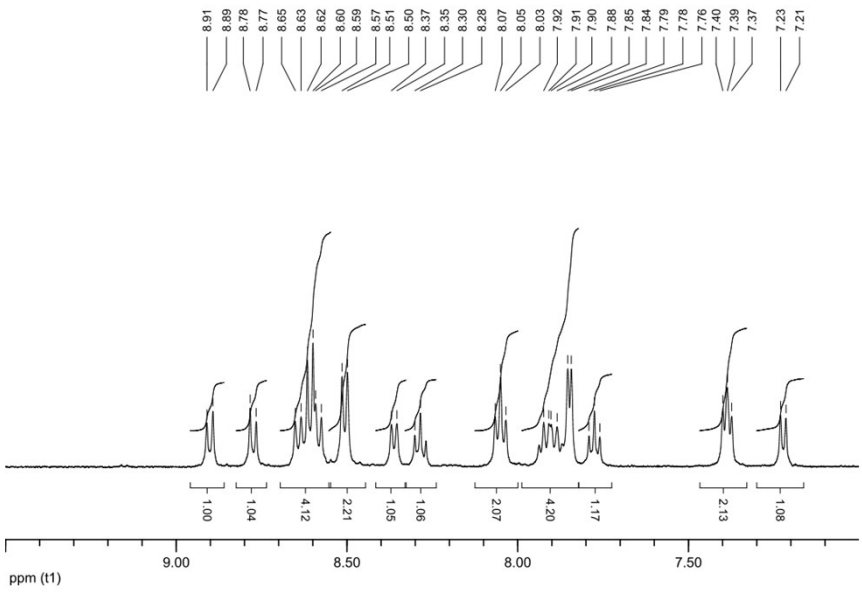

Figure S5A. ^{1}H NMR spectrum of *p*-[$\mathbf{2H_2O}$]Cl_2 in D_2O (80%) and CD_3OD (20%).

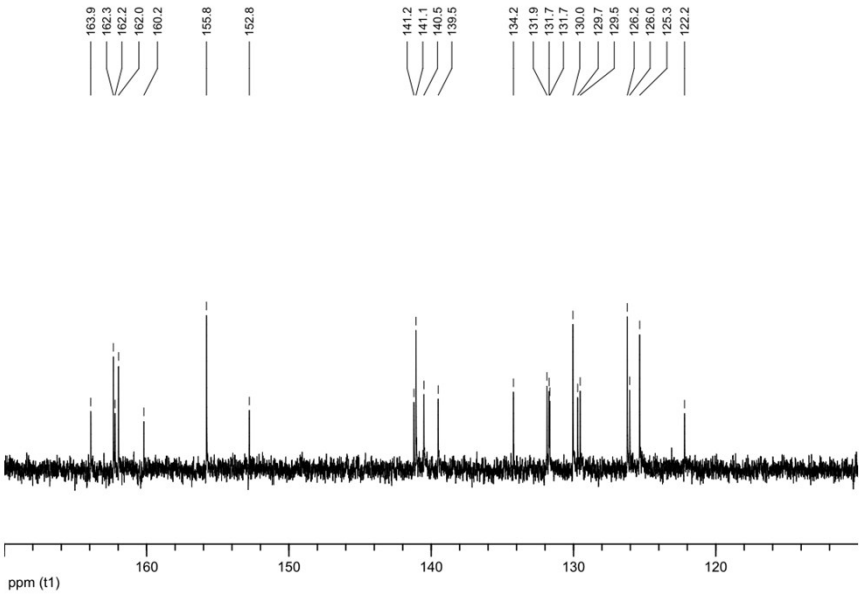

Figure S5B. ^{13}C NMR spectrum of *p*-[$\mathbf{2H_2O}$]Cl_2 in D_2O (80%) and CD_3OD (20%).

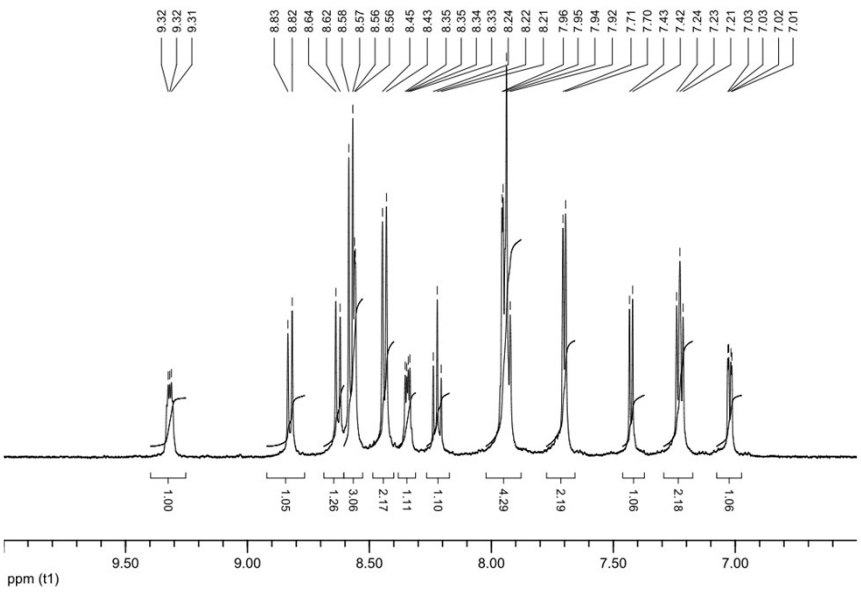

Figure S6A. ^{1}H NMR spectrum of *p*-[$\mathbf{3H_2O}$]Cl_2 in D_2O.

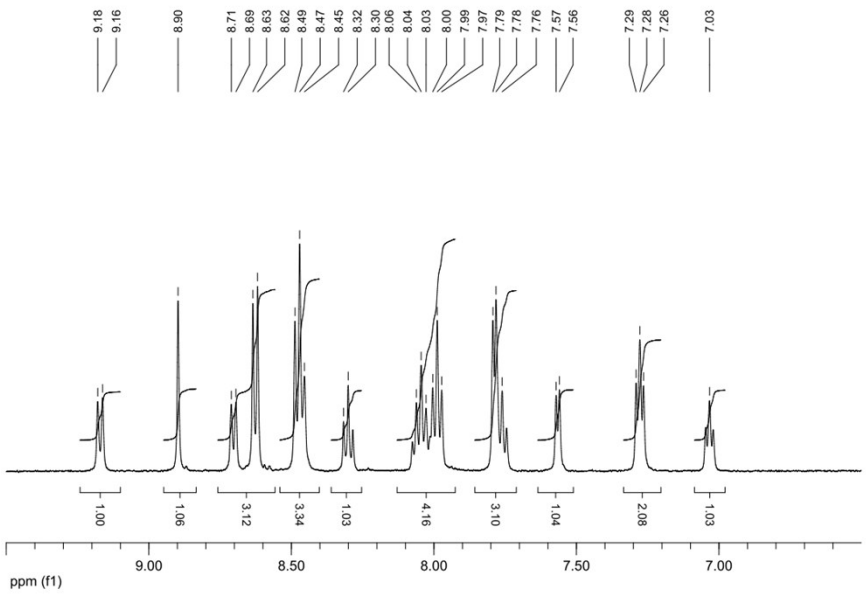

Figure S7A. ^{1}H NMR spectrum of *p*-[**4H$_2$O**]Cl$_2$ in D$_2$O.

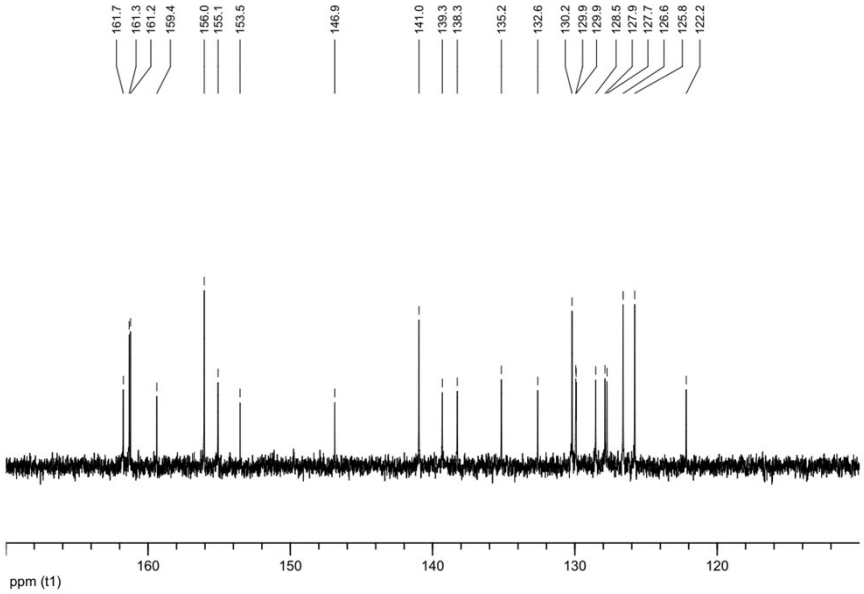

Figure S7B. ^{13}C NMR spectrum of *p*-[**4H$_2$O**]Cl$_2$ in D$_2$O.

Table S1. Selected crystallographic parameters

compounds	*p*-[**2Cl**](PF_6)	*p*-[**3Cl**](BF_4)	*p*-[**4Cl**](PF_6)·EtOH	*p*-[**2OH$_2$**](PF_6)$_2$·2H_2O	*p*-[**3OH$_2$**](CF_3SO_3)$_2$·H_2O	*p*-[**4OH$_2$**](NO_3)$_2$·2H_2O
empirical formula	$RuPF_6Cl_2N_5C_{29}H_{20}$	$RuBF_4Cl_2N_5C_{29}H_{20}$	$RuPF_6Cl_2N_5OC_{31}H_{26}$	$RuP_2F_{12}Cl_2N_5O_3C_{29}H_{26}$	$RuS_2F_6ClN_5O_8C_{31}H_{24}$	$RuClN_7O_9C_{29}H_{26}$
fw	755.45	697.30	801.51	919.01	909.19	753.09
radiation	Mo Kα	Mo Kα	Mo Kα	Mo Kα	Mo Kα	Mo Kα
crystal system	monoclinic	triclinic	monoclinic	triclinic	monoclinic	triclinic
space group	$P2_1/c$	$P\bar{1}$	$P2_1/c$	$P\bar{1}$	$P2_1/c$	$P\bar{1}$
a, Å	20.524(4)	7.7286(12)	8.7151(13)	9.010(2)	16.770(6)	8.599(3)
b, Å	8.2372(14)	12.0747(18)	13.061(2)	11.910(3)	17.343(7)	8.943(3)
c, Å	25.346(5)	14.592(2)	27.254(4)	18.237(6)	11.916(5)	20.080(6)
α, deg	90	81.760(2)	90	102.237(5)	90	77.361(3)
β, deg	137.909(3)	89.511(2)	94.409(2)	97.412(5)	101.073(6)	79.622(3)
γ, deg	90	77.947(2)	90	111.015(3)	90	89.260(4)
V, Å^3	2872.2(9)	1317.7(4)	3093.1(8)	1739.7(9)	3401(2)	1481.6(7)
Z	4	2	4	2	4	2
μ, mm^{-1}	0.858	0.858	0.804	0.724	0.755	0.682
T, K	293	100	100	100	100	100
d_{cal}, g/cm^3	1.747	1.7574	1.721	1.7504	1.776	1.643
T_{min}, T_{max}	0.4333, 1	0.647301, 1	0.427, 1	0.620, 0.986	0.9493, 0.9870	0.623220, 1
N_{ref}	6426	12164	7136	7682	7623	5319
$R[F^2 > 2\sigma(F^2)]$	0.0483	0.0312	0.0709	0.0628	0.0843	0.0707
$wR[F^2 > 2\sigma(F^2)]$	0.1080	0.0728	0.1983	0.1530	0.1839	0.2041
GOF	0.972	1.0393	0.907	1.0143	0.930	1.080

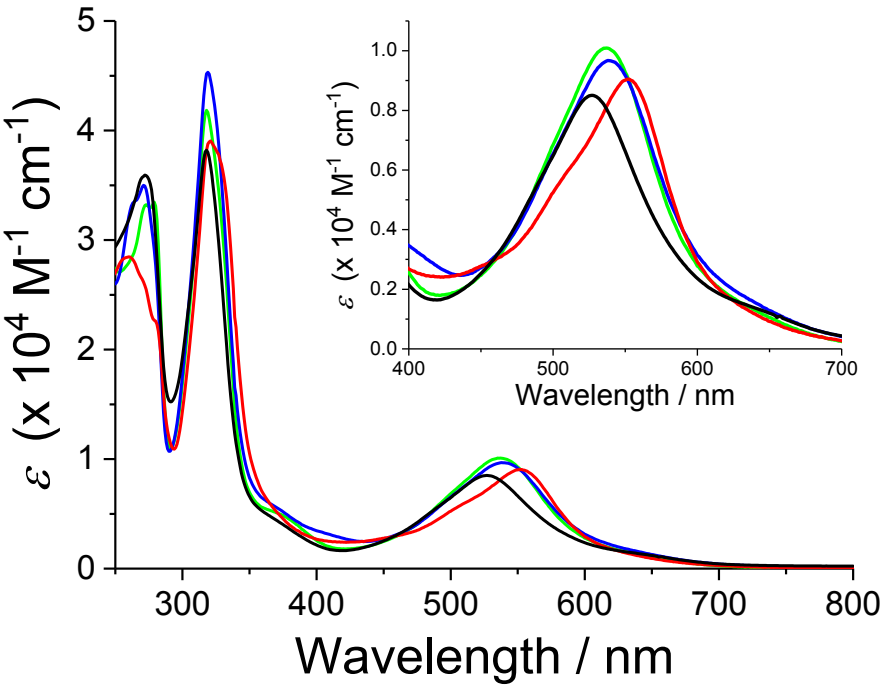

Figure S8. Absorption spectra of ruthenium complexes having R-pyqu ligands in methanol. *p*-**1Cl** (black), *p*-**2Cl** (red), *p*-**3Cl** (blue), and *p*-**4Cl** (green).

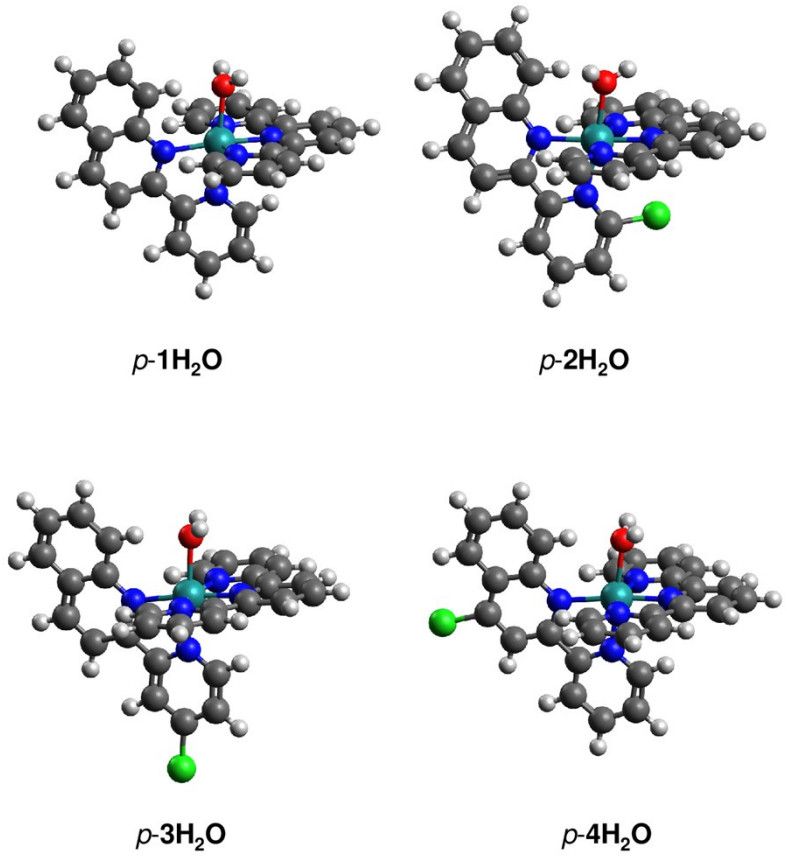

Figure S9 DFT optimized structures of *p*-**nH$_2$O** (n = 1-4), which were optimized at the B3LYP level of DFT using LanL2DZ basis set in Gaussian 09.

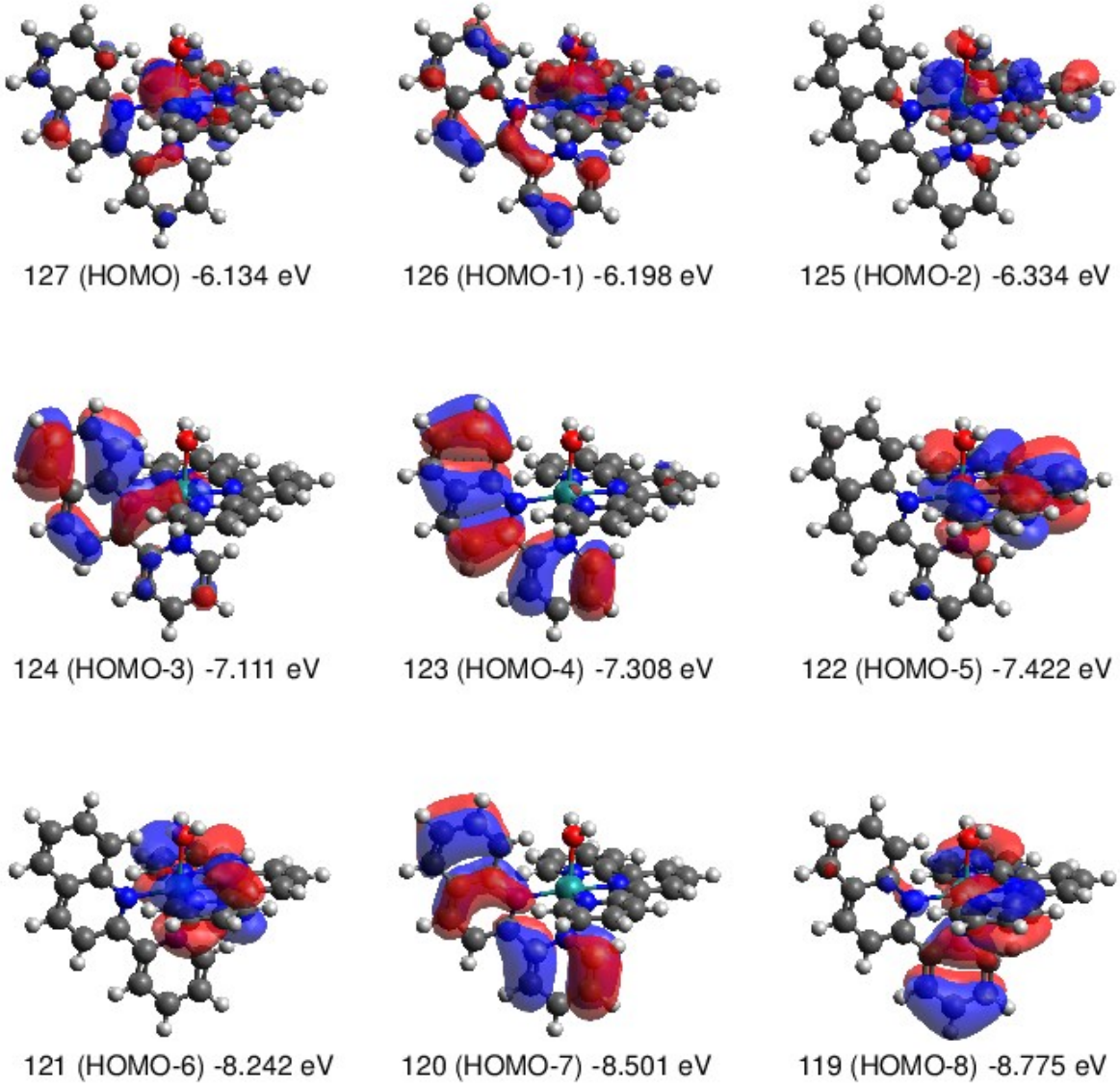

Figure S10 Frontier molecular orbitals of a fully optimized *p*-**1H$_2$O**. The structure was obtained by using B3LYP level of DFT and LANL2DZ basis set in Gaussian 09.

Figure S10 (Continued)

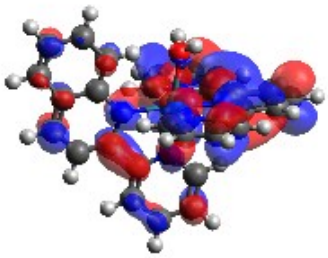

128 (LUMO) -2.911 eV

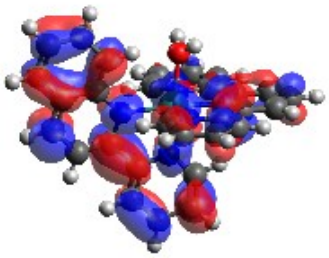

129 (LUMO+1) -2.865 eV

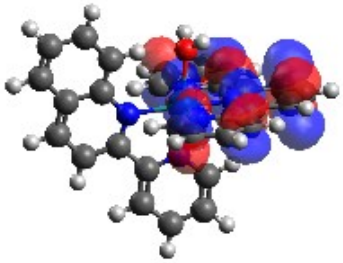

130 (LUMO+2) -2.637 eV

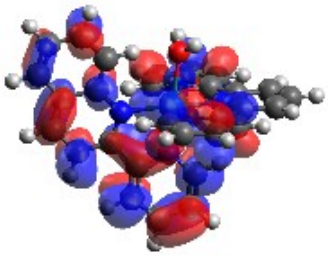

131 (LUMO+3) -1.789 eV

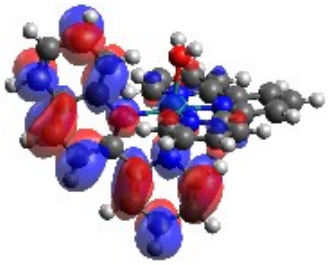

132 (LUMO+4) –1.747 eV

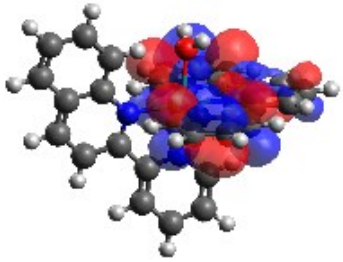

133 (LUMO+5) -1.700 eV

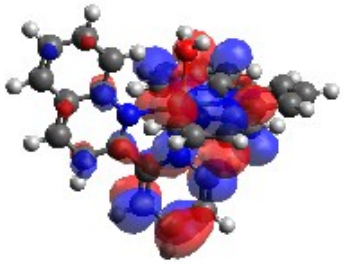

134 (LUMO+6) -1.558 eV

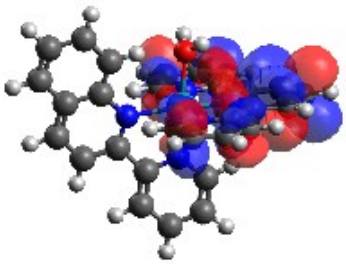

135 (LUMO+7) -0.919 eV

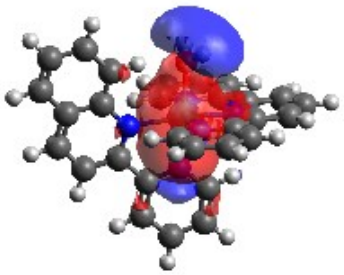

136 (LUMO+8) -0.794 eV

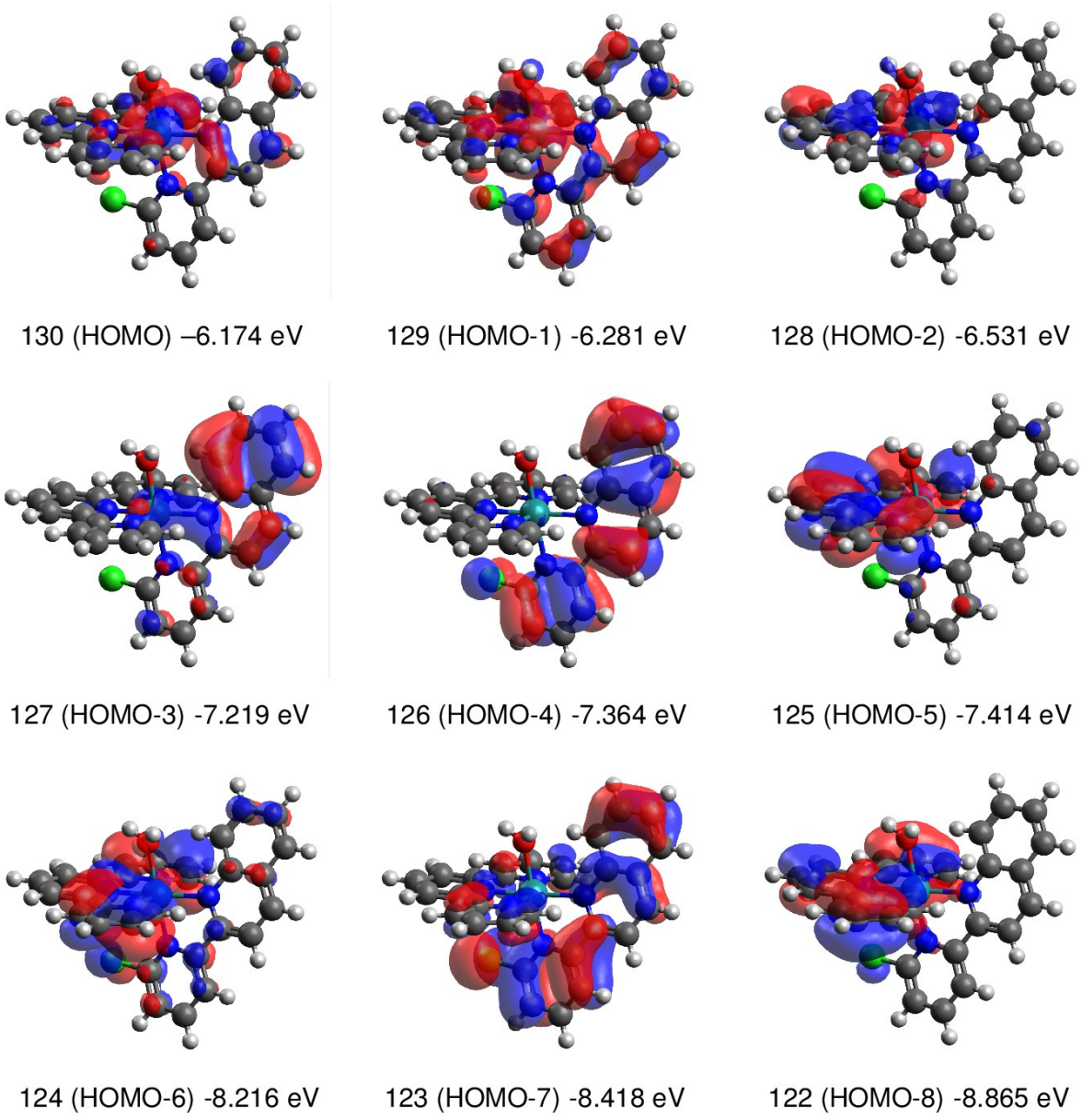

Figure S11 Frontier molecular orbitals of a fully optimized *p*-**2H$_2$O**. The structure was obtained by using B3LYP level of DFT and LANL2DZ basis set in Gaussian 09.

Figure S11 (Continued)

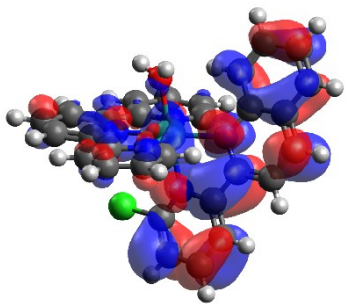

131 (LUMO) -3.082 eV

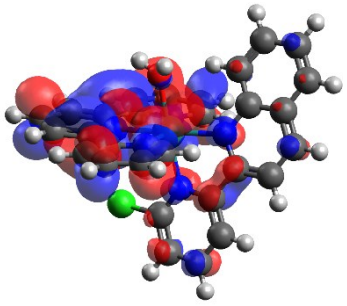

132 (LUMO+1) -2.862 eV

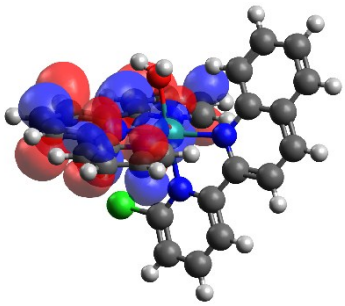

133 (LUMO+2) -2.628 eV

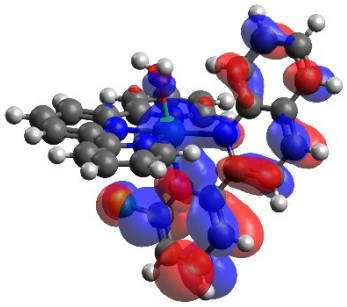

134 (LUMO+3) -1.974 eV

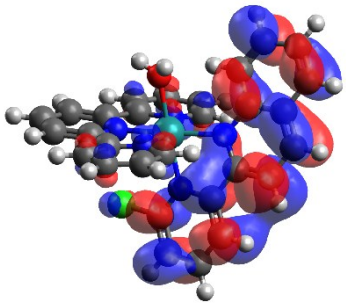

135 (LUMO+4) –1.881 eV

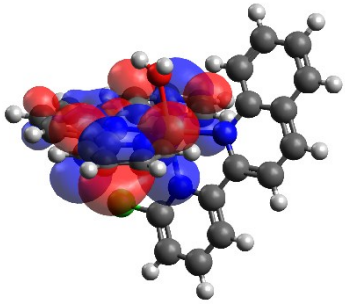

136 (LUMO+5) -1.698 eV

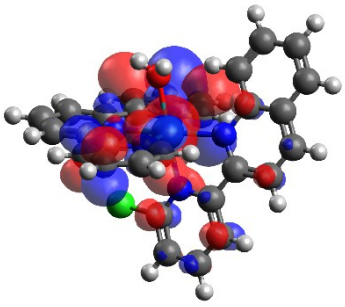

137 (LUMO+6) -1.639 eV

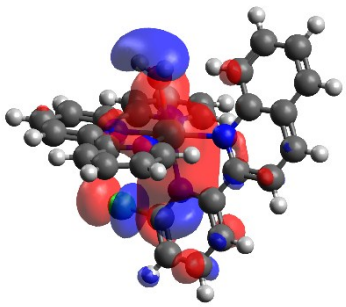

138 (LUMO+7) -1.132 eV

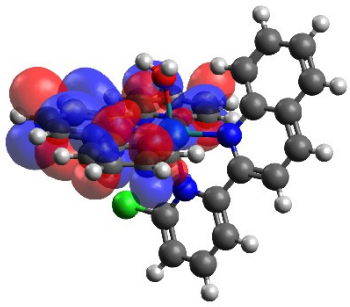

139 (LUMO+8) -0.917 eV

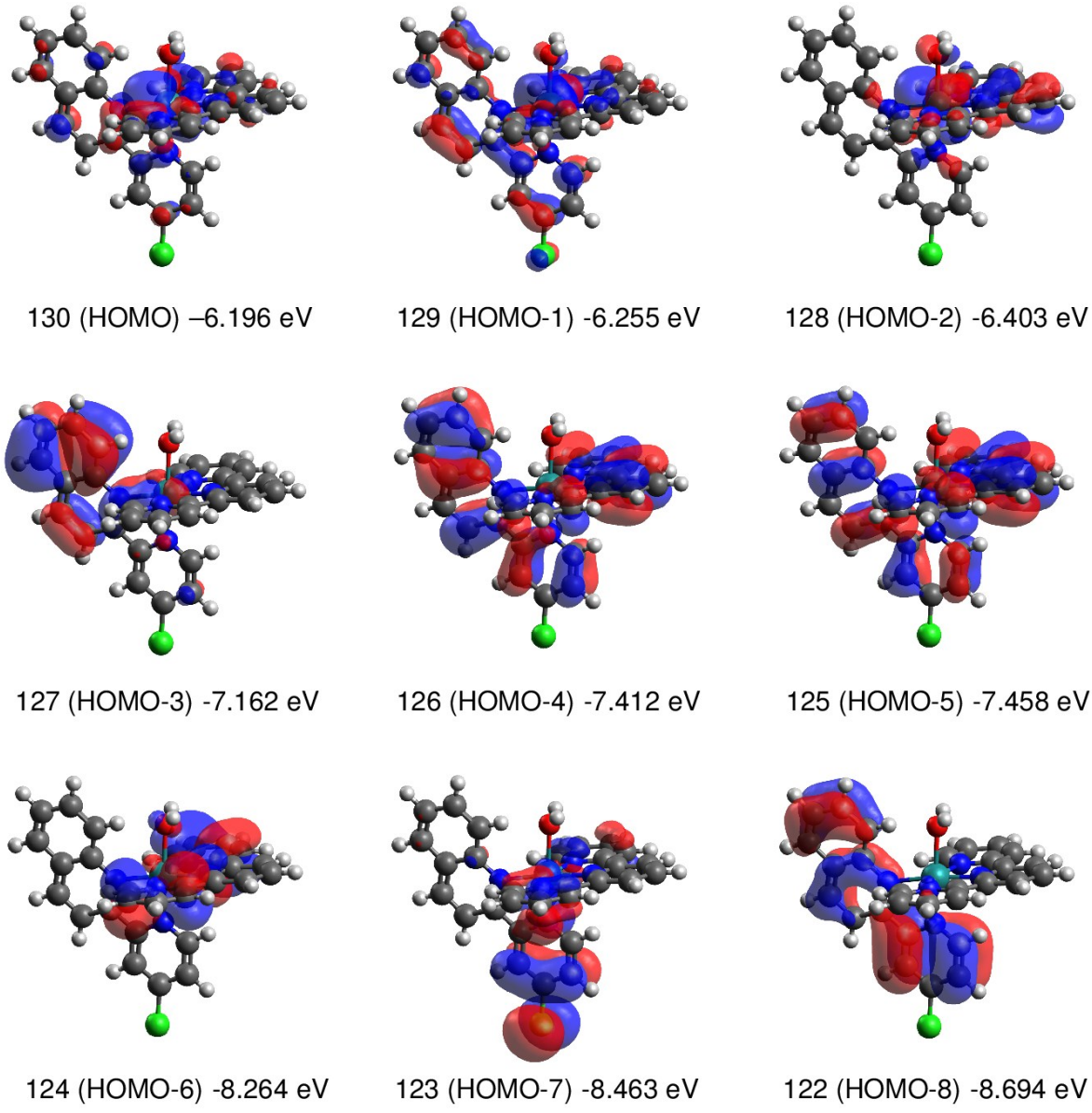

Figure S12 Frontier molecular orbitals of a fully optimized *p*-**3H$_2$O**. The structure was obtained by using B3LYP level of DFT and LANL2DZ basis set in Gaussian 09.

Figure S12 (Continued)

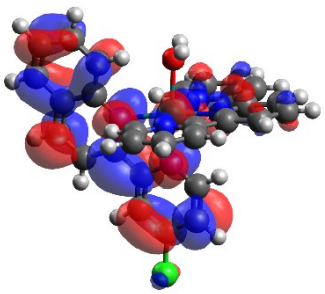

131 (LUMO) -3.018 eV

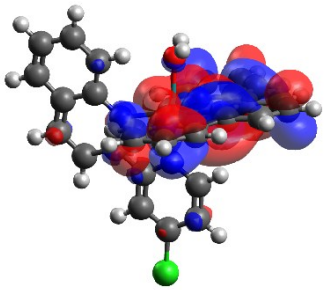

132 (LUMO+1) -2.922 eV

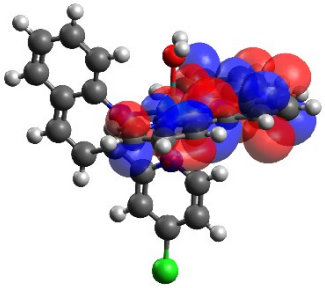

133 (LUMO+2) -2.660 eV

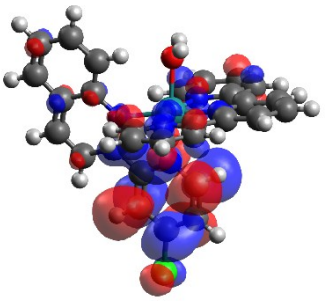

134 (LUMO+3) -1.979 eV

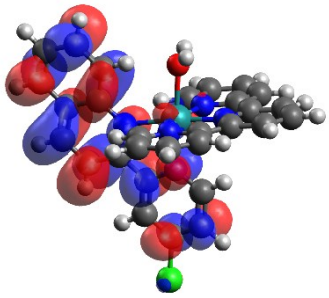

135 (LUMO+4) –1.851 eV

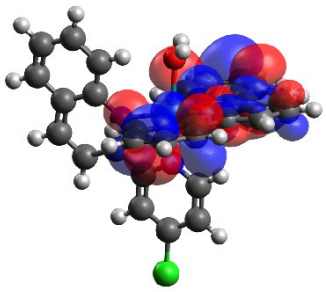

136 (LUMO+5) -1.720 eV

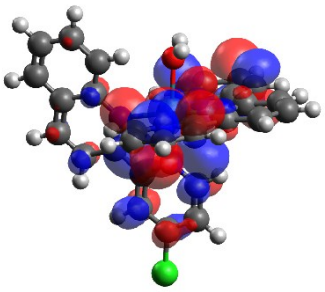

137 (LUMO+6) -1.631 eV

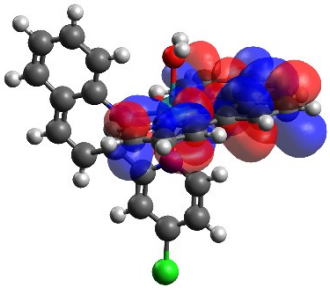

138 (LUMO+7) -0.940 eV

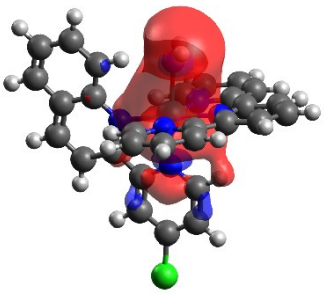

139 (LUMO+8) -0.841 eV

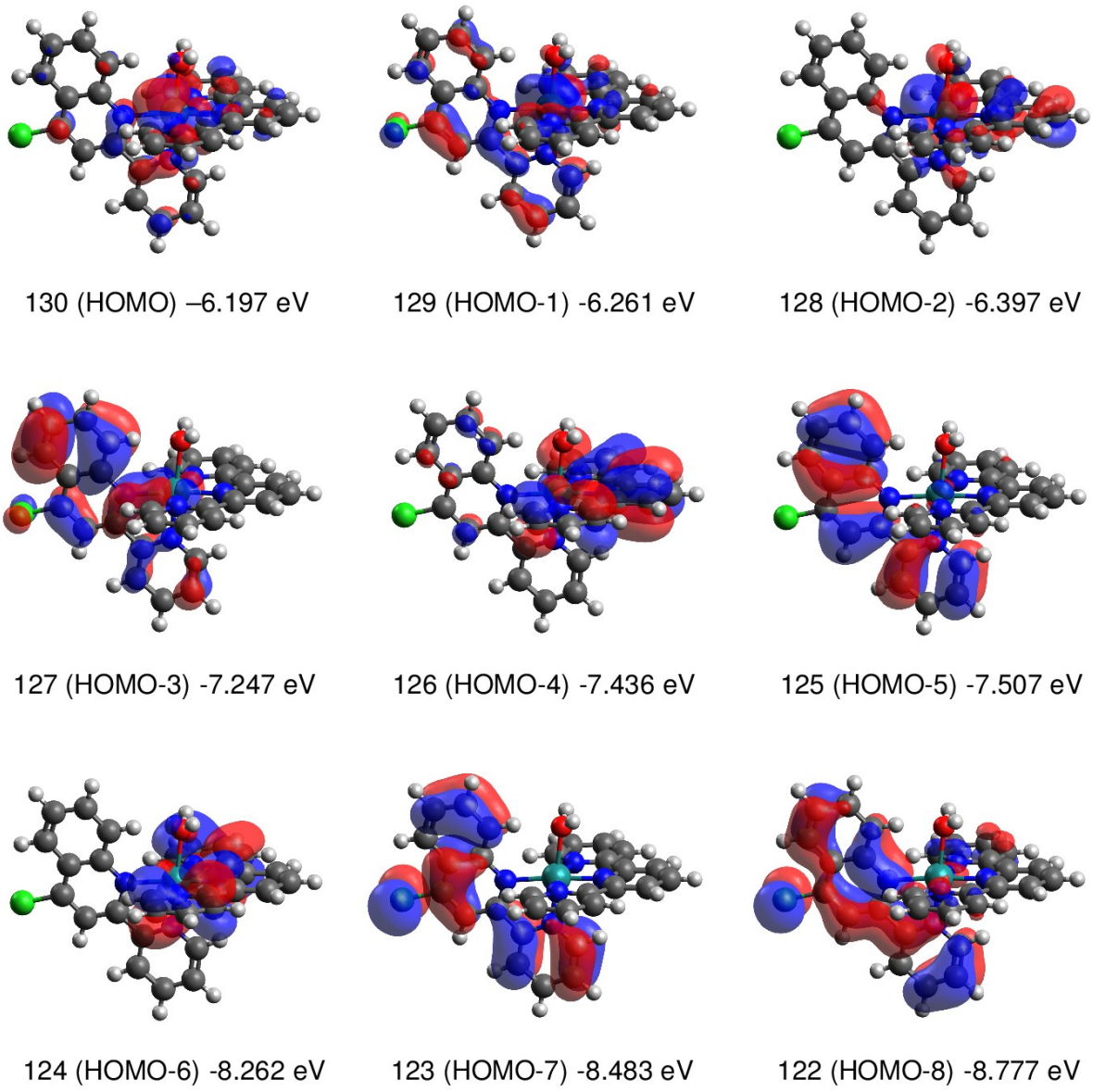

Figure S13 Frontier molecular orbitals of a fully optimized *p*-**4H$_2$O**. The structure was obtained by using B3LYP level of DFT and LANL2DZ basis set in Gaussian 09.

Figure S13 (Continued)

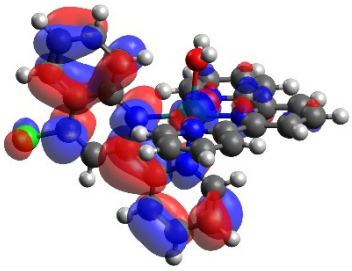

131 (LUMO) -3.032 eV

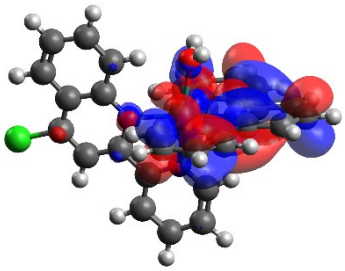

132 (LUMO+1) -2.921 eV

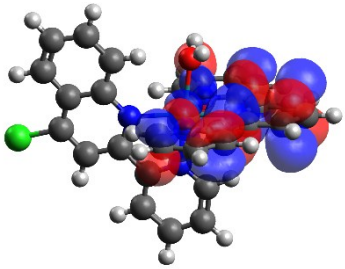

133 (LUMO+2) -2.658 eV

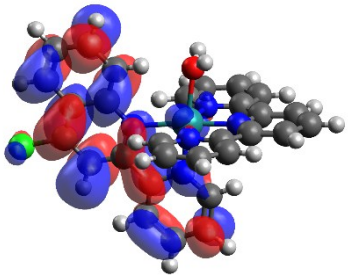

134 (LUMO+3) -1.996 eV

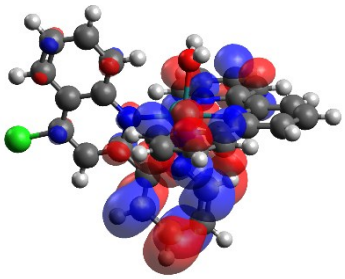

135 (LUMO+4) –1.817 eV

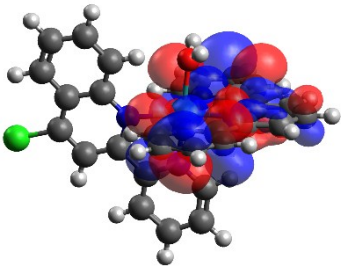

136 (LUMO+5) -1.718 eV

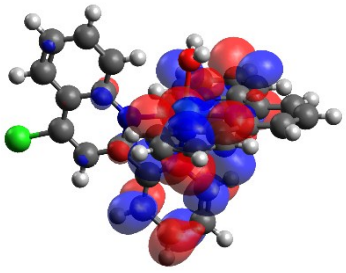

137 (LUMO+6) -1.599 eV

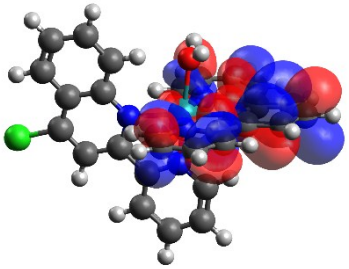

138 (LUMO+7) -0.937 eV

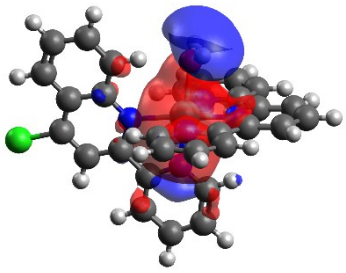

139 (LUMO+8) -0.833 eV

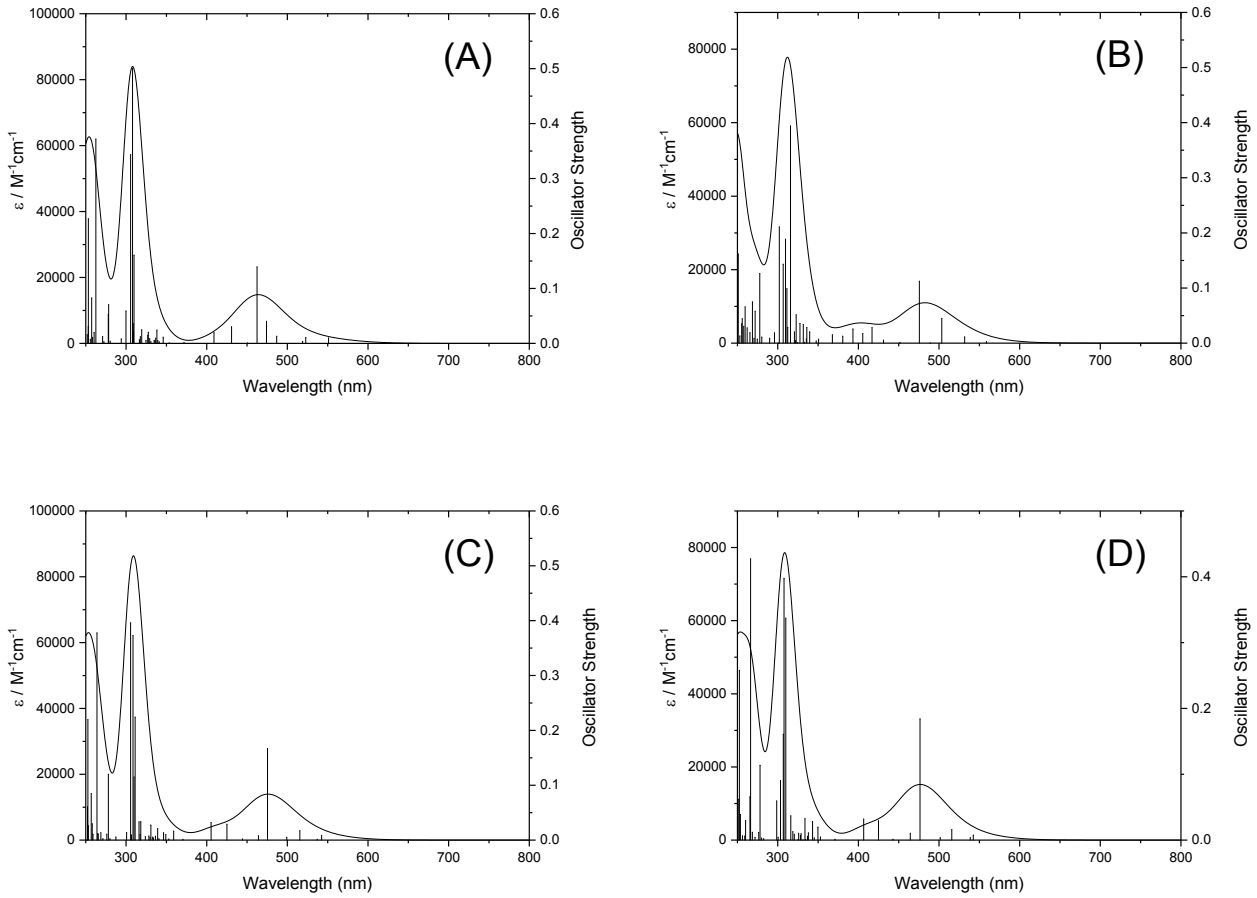

Figure S14 The calculated absorption spectra of *p*-**1H$_2$O** (A), *p*-**2H$_2$O** (B), *p*-**3H$_2$O** (C), and *p*-**4H$_2$O** (D) by using the time-dependent DFT calculations in PCM method (solvent: water). The singlet excitations, simulated with Gaussian functions, are shown as vertical bars with heights equal to oscillator strength.

Table S2. Selected list of TD-DFT energies of *p*-**1H$_2$O** (in water)

Excited State	λ/ nm	f	Major contributions
6	462.35	0.1392	H-1->LUMO (13%), H-1->L+1 (49%), HOMO->L+2 (28%)
27	309.80	0.1606	H-5->LUMO (12%), H-4->L+1 (16%), H-3->L+2 (10%), H-2->L+6 (20%), H-1->L+6 (10%)
30	308.06	0.5005	H-5->LUMO (34%), H-5->L+1 (12%), H-4->L+1 (12%)
31	305.56	0.3438	H-5->L+1 (46%), H-4->L+1 (12%)
32	299.85	0.0589	H-2->L+6 (21%), H-1->L+6 (35%), HOMO->L+6 (16%)
35	278.33	0.0703	H-5->L+2 (53%), HOMO->L+7 (25%)
36	277.91	0.0524	H-5->L+2 (31%), H-2->L+11 (14%), HOMO->L+7 (38%)
39	262.53	0.372	H-3->L+3 (14%), H-3->L+4 (39%), HOMO->L+9 (10%)
42	257.37	0.0828	H-3->L+3 (63%), H-3->L+4 (14%), HOMO->L+9 (11%)
44	253.20	0.2267	H-6->LUMO (33%), H-6->L+1 (17%), H-2->L+7 (16%)

Table S3. Selected list of TD-DFT energies of *p*-**2H$_2$O** (in water)

Excited State	λ/ nm	f	Major contributions
3	503.42	0.0448	H-1->LUMO (44%), H-1->L+1 (48%)
5	475.58	0.1123	H-2->L+1 (14%), H-1->LUMO (45%), H-1->L+1 (31%)
22	322.78	0.0515	H-5->LUMO (16%), H-1->L+5 (36%)
25	315.78	0.3942	H-4->LUMO (33%), H-1->L+3 (13%)
27	311.38	0.0986	H-4->L+1 (36%), H-2->L+4 (23%)
28	309.63	0.1885	H-5->L+1 (20%), H-4->L+1 (39%), H-2->L+5 (11%)
29	306.79	0.1432	H-5->L+1 (21%), H-2->L+6 (29%), H-1->L+6 (23%)
30	301.97	0.2108	H-5->L+1 (16%), H-2->L+5 (60%), H-2->L+6 (12%)
35	277.70	0.1264	H-5->L+2 (82%)
37	271.89	0.0579	H-6->LUMO (46%), HOMO->L+8 (16%)
39	268.57	0.0749	H-7->LUMO (16%), H-6->LUMO (25%), H-3->L+3 (20%), H-3->L+4 (11%)
42	259.54	0.0658	H-3->L+4 (32%), HOMO->L+9 (41%)
47	251.02	0.1615	H-4->L+3 (15%), H-3->L+4 (20%), H-1->L+9 (26%)
48	250.12	0.0839	H-7->L+1 (36%), H-2->L+8 (44%)

Table S4. Selected list of TD-DFT energies of *p*-**3H$_2$O** (in water)

Excited State	λ/ nm	f	Major contributions
5	475.43	0.1669	H-2->L+1 (31%), H-1->LUMO (59%)
27	311.19	0.2242	H-5->LUMO (22%), H-4->LUMO (14%), H-4->L+1 (36%)
28	309.83	0.1149	H-4->L+1 (26%), H-2->L+6 (20%), H-1->L+6 (12%)
29	308.59	0.373	H-5->LUMO (18%), H-4->L+1 (13%), H-2->L+6 (10%)
31	305.61	0.3961	H-5->L+1 (61%)
35	278.02	0.12	H-5->L+2 (60%), H-4->L+2 (26%)
41	263.87	0.3776	H-3->L+3 (23%), H-3->L+4 (30%)
44	256.74	0.0848	H-7->LUMO (28%), H-4->L+3 (30%), H-1->L+9 (15%)
46	252.65	0.2194	H-6->L+1 (20%), H-5->L+3 (19%), H-2->L+7 (23%)
47	252.13	0.061	H-6->L+1 (19%), H-5->L+3 (38%), H-4->L+3 (23%)

Table S5. Selected list of TD-DFT energies of *p*-**4H$_2$O** (in water)

Excited State	λ/ nm	f	Major contributions
5	476.40	0.1841	H-2->L+1 (31%), H-1->LUMO (62%)
27	310.01	0.3371	H-5->LUMO (46%), H-1->L+6 (10%)
28	307.83	0.3976	H-4->L+1 (44%), H-2->L+5 (11%), H-1->L+5 (10%)
29	306.87	0.1609	H-4->L+1 (14%), H-2->L+6 (26%)
30	303.38	0.0903	H-5->L+1 (89%)
32	298.74	0.0594	H-2->L+6 (20%), H-1->L+6 (28%), HOMO->L+6 (27%)
35	278.06	0.1136	H-4->L+2 (79%)
39	266.32	0.4272	H-6->LUMO (12%), H-3->L+3 (51%)
40	265.54	0.0656	H-6->LUMO (83%)
45	252.43	0.2579	H-6->L+1 (42%), H-2->L+7 (33%)
46	251.63	0.062	H-7->LUMO (11%), H-3->L+4 (71%)

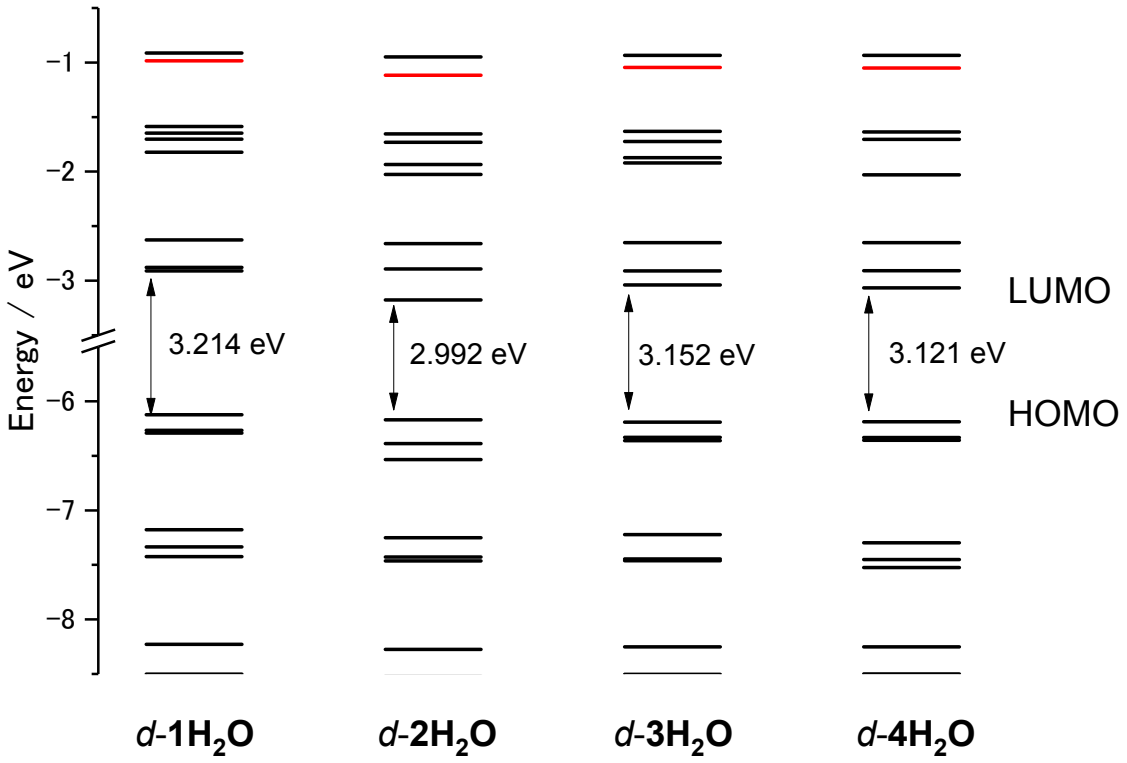

Figure S15. Energy level diagram of molecular orbitals of *d*-$\mathbf{nH_2O}$ (n= 1-4). The energy level of Ru-N antibonding dσ* orbitals (LUMO+7) are marked in red.

Table S6. Energies of optimized distal and proximal isomers (in water)

	Sum of energy at 298 K / Hartree		
Complex	proximal isomer	distal isomer	differences / kcal mol^{-1}
$1H_2O$	-1561.059453	-1561.055725	-2.34
$2H_2O$	-1575.389636	-1575.389304	-0.21
$3H_2O$	-1575.404388	-1575.400461	-2.46
$4H_2O$	-1575.403173	-1575.399308	-2.43